

# PhoMoH: Implicit Photorealistic 3D Models of Human Heads

Mihai Zanfir\*

Thiemo Alldieck\*

Cristian Sminchisescu

Google Research

## Abstract

We present *PhoMoH* [ˈfoʊ.moʊ], a neural network methodology to construct generative models of photorealistic 3D geometry and appearance of human heads including hair, beards, an oral cavity, and clothing. In contrast to prior work, *PhoMoH* models the human head using neural fields, thus supporting complex topology. Instead of learning a head model from scratch, we propose to augment an existing expressive head model with new features. Concretely, we learn a highly detailed geometry network layered on top of a mid-resolution head model together with a detailed, local geometry-aware, and disentangled color field. Our proposed architecture allows us to learn photorealistic human head models from relatively little data. The learned generative geometry and appearance networks can be sampled individually and enable the creation of diverse and realistic human heads. Extensive experiments validate our method qualitatively and across different metrics.

## 1. Introduction

The last two decades have witnessed significant efforts in modeling the human face and head, and considerable progress has been made [23]. Statistical models capturing a wide range of shapes, facial expressions, and sometimes appearances have been created [7, 41, 50, 68] and successfully deployed to a wide range of perception and synthesis tasks [24, 60, 61]. With the advent of deep learning, face and head models have more recently been used for synthetic data generation [66]. For this new use case, the generative properties of modern statistical models help create large corpora of training data that go well beyond the real data that has originally been used to train the models, in terms of human diversity of expression, head pose, and appearance. However, the current generation of models is still far from photorealistic – a shortcoming not only for synthesis, but also for inference. Additionally, most models capture only the face, or the head without hair, often lack appearance, and are of only medium spatial resolution. To alleviate such limitations, some methods combine statistical models with additional data such as textures, normal maps, (facial) hair, and accessories [66]. However, this approach usually requires significant manual work by artists. Moreover, the



Figure 1. Our implicit generative 3D head model *PhoMoH* enables disentangled control over a head’s geometry, pose and shape, as well as appearance and facial expressions. On the first row, we show a random sample altered using all factors. On the second row, we augment a scan that has been embedded in our model.

models are not completely learned from data, and are thus hard to scale. When aiming for a diverse holistic model of the human head, the majority of current models additionally face the technical barrier of relying on a template mesh with fixed topology. In practice this means, that *by design*, in the absence of additional components, the models are not easily capable of capturing (facial) hair, clothing, or head shapes which deviate from a generic template. In this work, we propose to use implicit function networks to go beyond such limitations. Implicit function networks [17, 43, 47], an instance of neural fields [67], model a shape by a decision boundary, or level-set, of a function over points in space. Consequently, no predefined explicit shape template is used, and the networks can represent varying topology. This property is particularly useful for modeling the above mentioned desired features, such as hair or accessories, which are missing in the majority of state-of-the-art models. On the other hand, the current models do have desirable properties, as *e.g.* well-covered face geometry or expression spaces. To this end, we propose to re-use an existing model and augment it with missing features, instead of going through the laborious and potentially error-prone process of learning a model from scratch. This way we ensure that our model is on par with state-of-the-art in terms of expressiveness and is capable of additional coverage. Concretely, we build upon the head component of *imGHUM* [3] a recent implicit, Signed Distance Function (SDF)-based version of the statistical body model *GHUM* [68]. *GHUM* and *imGHUM* can be controlled by a set of generative latent representations for head pose, head shape, and facial expressions, respectively. Aiming towards photorealism, we augment *imGHUM* with

\* The first two authors contributed equally.

an additional layer that captures missing factors. Our joint model, PhoMoH, introduces control over high-resolution geometry including wrinkles and (facial) hair, which we refer to as *identity*. Additionally, PhoMoH benefits from a detailed, local geometry-aware, and semantically coherent *appearance* model trained using a novel perceptual loss.

To enable PhoMoH’s properties, we further introduce a number of *technical contributions*. *First*, we propose a dual Variational Autoencoder architecture and a training procedure to produce disentangled latent representations for identity and appearance with an imposed Gaussian prior. This enforces compactness and enables latent sampling, interpolation, and optimization. *Second*, we propose a novel perceptual patch loss with importance sampling to improve the visual fidelity of our results. *Finally*, we introduce a local geometry feature, trained without explicit supervision, thus enabling interesting applications beyond its original use-case of semantically coherent surface coloring. In summary, we propose PhoMoH, an implicit, photorealistic head model, with control over facial expression, head pose, low-dimensional head shape, and high-resolution geometric identity and appearance detail (see Fig. 1).

## 2. Related Work

Following the ground-breaking work of Blanz and Vetter [7], the realism and the generation capabilities of 3D morphable face and head models (3DMMs) have steadily increased [23]. Two distinct lines of works in this space exist, based on (1) explicit mesh-based geometry, and (2) neural implicit surface-based modeling. The mesh-based representation is by far the most popular in this space, with the implicit one only recently coming into spotlight.

**Explicit Models.** A plethora of *face models* have been developed and proposed over the years, all having their roots in the seminal work [7], where a low dimensional space is learned for both the appearance and the geometry of the face by using PCA. Subsequent work [2, 8–10, 12, 24, 27, 37, 50, 62, 64] have expanded on this approach by using better quality or more accessible training data, better registration techniques, or producing more expressive models. More related are *head models*, that also have seen a rapid development over the years. One of the earliest models, FLAME [41], was trained on 3D head scans, and has decoupled geometric linear latent spaces for shape, pose, and facial expressions. [20, 21] introduce a 3D morphable linear model for shape and texture of the full human head. [52, 53] expand on this work to build a more detailed model, with PCA-based controls for the face, cranium, ears and eyes, and basic modeling of the teeth, tongue and inner mouth cavity, as well as an image-based texture completion pipeline. There are also a number of full body statistical models that support the independent control of the head shape, pose, and expression such as SMPL-X [49],

Frank/Adam [36], and GHUM [68]. For the latter, an implicit formulation, named imGHUM [3], was presented as well, which we build upon in this work. It is important to note that none of these models are able to represent geometry and/or color for hair or accessories.

**Implicit Models** for 3D reconstruction and generation of diverse objects have been introduced in [17, 43, 47]. In [47], a generative auto-decoder based continuous SDF representation is proposed. Different from an auto-encoder, whose latent code is produced by an encoder, an auto-decoder directly accepts a latent vector as input. A random latent vector is assigned to each data point in the beginning of training, and the latent vectors are optimized together with the decoder weights. Implicit models have been quickly adopted for 3D human full body reconstruction [4, 18, 31, 34, 56] and modeling [22, 44, 45]. In the context of modeling 3D faces and heads, a few approaches have been explored in recent work and are the most related to ours. i3DMM [72] is a deep implicit 3D morphable model of the full head with learned latent spaces for geometry and color. The full geometric code is decomposed into local codes controlling identity, expression and hairstyle, while the full color code is further decomposed into identity and hairstyle. Their architectures supports the disentanglement between different latent factors, but does not allow the color field to be informed by semantic signals associated with the underlying geometric field. This limits the plausibility of samples, as for example ear colors could appear splattered onto hair geometry. One additional drawback is the fact that geometry is not metric, limiting some of the practical applications. NPHM [28] is a recent implicit head model, represented using an ensemble of local neural fields. However, NPHM only models the geometry and heavily relies on non-rigid registration to a template mesh. In contrast, our method bypasses this complex pre-processing step inherited from mesh-based models and additionally models disentangled appearance. ImFace [75] learns a nonlinear implicit representations of only the face geometry, with control over the identity and expression. Related is also LISA [19], an implicit generative hand model with disentangled shape, pose and appearance parameters. HeadNerf [35] is a neural radiance field (NeRF)-based [46] head model that integrates NeRF with a parametric representation of the human head. Like in most NeRF-based approaches, plausible geometry is not guaranteed. In recent work, MoRF [63] learns highly detailed radiance fields of human heads and allows morphing between identities. In contrast, our method produces actual 3D geometry (instead of only images) and allows for sampling diverse 3D heads.

**Building personalized 3D face or head avatars** from a few images [11, 13, 38, 55], or monocular video [14, 25, 26, 29, 76] of an individual is a *related but complementary line of work*, which often relies on a statistical model for recon-

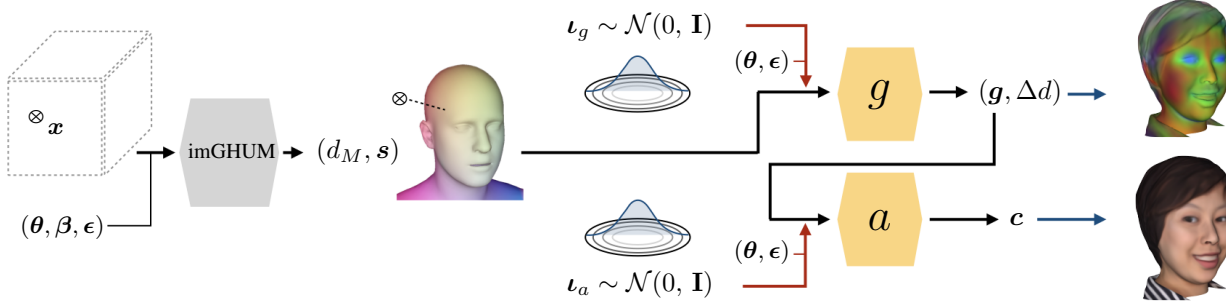


Figure 2. Overview of our method. We use imGHUM to canonicalize points in space  $\mathbf{x}$  into the pose, shape, and expression-zero-space  $(d_M, \mathbf{s})$ . The geometry network  $g$  computes signed distance updates  $\Delta d$  to the distance  $d_M$  returned by imGHUM.  $g$  additionally returns a geometric feature  $\mathbf{g}$  that is input to the appearance network  $a$  returning a color  $\mathbf{c}$  for  $\mathbf{x}$ . We sample identities by using learned normal distributed latent codes for geometry  $\boldsymbol{\iota}_g$  and appearance  $\boldsymbol{\iota}_a$ , respectively (red arrows). Using Marching Cubes (blue arrows), we can extract meshes from  $g$  and  $a$ .

struction, or as basic representation to further personalize. For instance, H3D-Net [55] presents an implicit model for 3D head reconstruction from a few images, with a coarse geometric prior trained on a rich dataset of 3D head scans. NeRF-based models have been also used for personalization, either to represent the full person [40, 42, 51, 65, 69] or by focusing on the head [5, 25, 48]. In contrast to our work, all these methods estimate personalized 3D heads or faces of individuals, do not build a statistical model, and do not allow for the generation of novel identities. Our model could also be used in a personalization process, either as a statistical prior or as a base representation to further refine. Also worth mentioning are 3D-aware GAN models [15] that produce realistic synthesized images with inaccurate 3D frontal geometry and have limited controllability.

### 3. Background

Our model builds on top of imGHUM [3], an implicit model of human pose, shape, and facial expression. imGHUM is an implicit SDF-based model compatible with the explicit mesh-based model GHUM [68], meaning it shares the same low-dimensional parameterization. GHUM and imGHUM model the human body without hair or high-resolution details such as fine wrinkles and also lack an appearance model. imGHUM is composed of four sub-models for critical parts of the human body – please see the original paper for details. We use the sub-model for the head as the base representation for PhoMoH and simply refer to it as imGHUM hereafter. imGHUM is a function over a point space  $\mathbf{x}$ , the head pose  $\boldsymbol{\theta}$ , the low-dimensional head shape  $\boldsymbol{\beta}$ , and the facial expression  $\boldsymbol{\epsilon}$ , returning the signed distance  $d_M$  at  $\mathbf{x}$  w.r.t. the model’s surface. Further, imGHUM returns  $\mathbf{s} \in \mathbb{R}^3$ , the nearest neighbor of  $\mathbf{x}$  on the surface represented as coordinates on a reference mesh. Inspired by [69], we use imGHUM as a function mapping  $\mathbf{x}$  into a reference frame defined through  $(d_M, \mathbf{s})$  and learn our model in this reference frame. We illustrate the mapping into  $(d_M, \mathbf{s})$ -space by looking at a concrete example: While the tip of the nose will be located at different points in space

$\mathbf{x}$  depending on the head pose or shape, it will always be mapped to the same  $(d_M, \mathbf{s})$  code. This is similar to mesh-based modeling, where the tip of the nose will always be modeled by the same vertex. By building our model in the  $(d_M, \mathbf{s})$ -space, we exploit two properties from imGHUM: (1) our model does not need to learn the range of human shapes, poses, and expression, since these are already well covered by imGHUM and (2) imGHUM serves as an implicit canonicalization function allowing us to learn from pairs of imGHUM codes and unstructured 3D data.

### 4. Method

We use template-free neural fields to model both geometry and appearance for human heads. Our model is controlled by disentangled factors  $\mathcal{Z} = (\boldsymbol{\theta}, \boldsymbol{\beta}, \boldsymbol{\epsilon}, \boldsymbol{\iota}_g, \boldsymbol{\iota}_a)$ , including head pose  $\boldsymbol{\theta}$ , low-dimensional head shape  $\boldsymbol{\beta}$ , facial expression  $\boldsymbol{\epsilon}$ , geometric identity  $\boldsymbol{\iota}_g$ , and appearance  $\boldsymbol{\iota}_a$ . Concretely, we model the human head as a function over a point in space  $\mathbf{x}$  returning the signed distance  $d$  at  $\mathbf{x}$  w.r.t. the head surface, together with its color  $\mathbf{c}$ . The surface  $\mathcal{S}$  of the head is implicitly defined by the zero-level-set of the distance-field modeled by the neural-network  $f$  parameterized by network weights  $\phi$

$$\mathcal{S}_\phi(\mathcal{Z}) = \left\{ \mathbf{x} \in \mathbb{R}^3 \mid f(\mathbf{x}, \mathcal{Z}; \phi) = (0, \mathbf{c}) \right\}. \quad (1)$$

At test-time we want to be able to sample different appearances for a given geometry. Thus, we decompose  $f$  into the two multilayer perceptrons (MLPs)  $g$  modeling the geometry, and  $a$  modeling the appearance. However, we argue that appearance should follow the semantics defined by geometry. For example, skin color should be only placed on skin structure, whereas hair color should only be returned for regions corresponding to hair. This means that while appearance should be disentangled from specific geometric identities, it should still be informed by the semantic structure defined by  $g$ . To this end, we condition  $a$  on a low-dimensional surface descriptor  $\mathbf{g}$  instead of a point  $\mathbf{x}$ .  $\mathbf{g}$  is an additional output of  $g$  and is learned without explicit supervision. This is in a similar spirit as the global

geometry feature vector in IDR [71]. While IDR performs per object optimization and shows appearance transfer only for uniform materials, our surface descriptor  $\mathbf{g}$  allows for complex and semantically meaningful coloring of a whole object class. Moreover, we also apply layer normalization (LN) to  $\mathbf{g}$  before passing it to the appearance network. In practice this is helpful to prevent information leakage from the geometric identity code into the appearance network and thus helps to disentangle the model parameters, as we will show. Besides being a local descriptor for appearance,  $\mathbf{g}$  is additionally useful for various applications, see Sec. 5.4. Finally, we learn our model in unposed, neutral expression, and mean-shape space, which we achieve by canonicalizing  $\mathbf{x}$  to  $(d_M, \mathbf{s})$  using imGHUM  $M$ . The distance returned by imGHUM  $d_M$  is a good approximation of the true surface distance  $d$ , thus we let  $g$  only find a residual distance  $\Delta d$ . The full model  $f$  reads as

$$f(\mathbf{x}, \mathcal{Z}; \phi) = (d_M + \Delta d, \mathbf{c}) = (d, \mathbf{c}), \quad (2)$$

with

$$a(LN(\mathbf{g}), \boldsymbol{\nu}_a, \boldsymbol{\theta}, \boldsymbol{\epsilon}; \phi_a) = \mathbf{c}, \quad (3)$$

$$g(d_M, \mathbf{s}, \boldsymbol{\nu}_g, \boldsymbol{\theta}, \boldsymbol{\epsilon}; \phi_g) = (\Delta d, \mathbf{g}), \quad (4)$$

$$M(\mathbf{x}, \boldsymbol{\theta}, \boldsymbol{\beta}, \boldsymbol{\epsilon}) = (d_M, \mathbf{s}). \quad (5)$$

We additionally condition  $g$  and  $a$  on pose  $\boldsymbol{\theta}$  and expression  $\boldsymbol{\epsilon}$  to capture pose and expression dependent geometry and appearance variations not modeled by imGHUM. See Fig. 2 for an overview. In the following we will use  $d_{\mathbf{x}}$  as shorthand notation for the distance,  $\mathbf{g}_{\mathbf{x}}$  for the geometric feature and  $\mathbf{c}_{\mathbf{x}}$  for the color returned by  $f$  (or  $g$ , respectively) at point  $\mathbf{x}$ , and drop the dependence on  $\mathcal{Z}$  and  $\phi$  for clarity.

The latent codes for geometric identity  $\boldsymbol{\nu}_g$  and appearance identity  $\boldsymbol{\nu}_a$  are unknown before the model is trained. We use auto-decoding [47] to obtain optimal latent representations. In this set-up, training pairs of shapes and random latent codes are formed. During training, the latent codes are updated together with the model weights. In contrast to prior work, we additionally enforce a Gaussian prior on  $\boldsymbol{\nu}_g$  and  $\boldsymbol{\nu}_a$ . This guarantees *i.a.* that we can effectively draw samples from both latent codes during test time. In such a setup, referred to as Variational Autodecoder (VAD) [32, 73], one uses the reparameterization trick from Variational Autoencoders (VAEs) [39]: instead of directly learning the latent codes, one represents them with the parameters of the approximate posterior distribution, concretely a mean and a standard deviation vector  $\boldsymbol{\mu}$  and  $\boldsymbol{\sigma}$ . During training, random latent codes are sampled based on those.

We have now defined all components of our implicit head model  $f$ . To train  $f$ , we minimize a number of loss functions, defined in the sequel, w.r.t. the model weights  $\phi$  and the mean and standard deviation vectors of the latent embeddings  $\boldsymbol{\nu}_g$  and  $\boldsymbol{\nu}_a$ .

#### 4.1. Losses

For training we require pairs of 3D head scans together with imGHUM parameters approximating the scan; Sec. 4.2 gives details on how to obtain those. We start by defining losses for the geometry, and continue with losses for the appearance, as well as regularizers.

**Geometry.** Given a set of points  $\mathcal{O}$  on a ground truth mesh  $\mathcal{M}$  describing the surface  $\mathcal{S}$  together with its ground truth surface normals  $\bar{\mathbf{n}}$ , and corresponding imGHUM parameters  $(\boldsymbol{\theta}, \boldsymbol{\beta}, \boldsymbol{\epsilon})$  approximating  $\mathcal{M}$ , we minimize

$$\mathcal{L}_g = \frac{1}{|\mathcal{O}|} \sum_{i \in \mathcal{O}} \lambda_g |d_{\mathbf{x}_i}| + \lambda_n \|\mathbf{n}_{\mathbf{x}_i} - \bar{\mathbf{n}}_i\|, \quad (6)$$

where  $\mathbf{n}_{\mathbf{x}} = \nabla_{\mathbf{x}} d_{\mathbf{x}}$  is the estimated surface normal defined by the gradient of the estimated distance w.r.t.  $\mathbf{x}$  and  $\lambda_*$  weight the different loss components. Further, we supervise the SDF with the Eikonal loss [31] for points  $\mathcal{F}$  around the surface and additionally supervise their sign

$$\mathcal{L}_e = \frac{1}{|\mathcal{F}|} \sum_{i \in \mathcal{F}} (\|\mathbf{n}_{\mathbf{x}_i}\| - 1)^2 \quad (7)$$

$$\mathcal{L}_l = \frac{1}{|\mathcal{F}|} \sum_{i \in \mathcal{F}} \text{BCE}(l_i, \psi(kd_{\mathbf{x}_i})), \quad (8)$$

based on binary sign labels  $l$ , sigmoid function  $\psi$ , binary cross-entropy BCE, and the learnable parameter  $k$  controlling the sharpness of the decision boundary.

**Appearance.** For all points, we supervise the color component of  $f$  to match the ground truth color  $\bar{\mathbf{c}}$  of the nearest neighbor on the surface of  $\mathcal{M}$

$$\mathcal{L}_c = \frac{1}{|\mathcal{O} \cup \mathcal{F}|} \sum_{i \in \mathcal{O} \cup \mathcal{F}} |\mathbf{c}_{\mathbf{x}_i} - \bar{\mathbf{c}}_i|. \quad (9)$$

While  $\mathcal{L}_c$  is theoretically sufficient to supervise the color field, in practice training only using  $\mathcal{L}_c$  leads to overly smooth results. To this end, we propose a novel perceptual patch loss with importance sampling to improve the visual fidelity of results. We sample a patch by first sampling a point on the mesh. Next, we create a virtual camera viewing the sampled point along its surface normal. Using this camera, we render a small image and additionally compute the 3D surface locations corresponding to each pixel – see Sec. 4.2 for details. For all 3D points in the resulting patch  $\mathcal{P}$  and the corresponding rendered image  $\bar{\mathbf{I}}^{\mathcal{P}}$ , we enforce the previously introduced color and distance losses, and additionally apply a VGG-loss [16] for an image  $\mathbf{I}^{\mathcal{P}}$  formed using the colors returned by  $f$  for all  $\mathbf{x} \in \mathcal{P}$

$$\mathcal{L}_p = \frac{1}{|\mathcal{P}|} \sum_{i \in \mathcal{P}} \left( \lambda_{pc} |\mathbf{c}_{\mathbf{x}_i} - \bar{\mathbf{I}}_i^{\mathcal{P}}| + \lambda_{pd} |d_{\mathbf{x}_i}| \right) + \lambda_{pp} \text{VGG}(\mathbf{I}^{\mathcal{P}}, \bar{\mathbf{I}}^{\mathcal{P}}), \quad (10)$$

where  $\bar{\mathbf{I}}_i^{\mathcal{P}}$  is the  $i$ -th pixel color in the ground truth rendered patch. In contrast to rendering losses proposed in prior work [4, 71], our perceptual patch loss does not require memory or computationally expensive differentiable



Figure 3. Random heads sampled from our model trained on the LHS dataset showing varying head shape, expression, geometric identity, and appearance. For each sample, we show 3D geometry and appearance side-by-side.

rendering strategies, and all the expensive operations can be performed during data pre-processing.

**Regularization.** To enforce a Gaussian prior on  $\iota_g$  and  $\iota_a$ , we minimize the Kullback-Leibler (KL) divergence loss [39] for each mean and standard deviation pair  $(\sigma, \mu)$  corresponding to each instance of  $\iota_g$  and  $\iota_a$

$$\mathcal{L}_{\text{KL}} = -\frac{1}{2} \sum_{j=1}^J (1 + \log(\sigma_j^2) - \mu_j^2 - \sigma_j^2), \quad (11)$$

where  $j$  references the  $j$ -th dimension.

We use pairs of meshes  $\mathcal{M}$  and imGHUM parameters  $(\theta, \beta, \epsilon)$  approximating  $\mathcal{M}$  during training – see Sec. 4.2. Since we do not have access to ground truth imGHUM parameters, we allow our model to “correct” those estimates  $(\theta, \beta, \epsilon)$  during training. To this end, we treat  $(\theta, \beta, \epsilon)$  as pre-initialized variables and update those together with model weights and latent representations. We further guide the optimization using 3D facial keypoints  $\mathcal{K}$  leveraged to initialize the imGHUM parameters (*cf.* Sec. 4.2)

$$\mathcal{L}_k = \frac{1}{|\mathcal{K}|} \sum_{i \in \mathcal{K}} |d_{k_i}| + |s_{k_i} - \bar{s}_i|, \quad (12)$$

where  $s$  are reference points returned by imGHUM and  $\bar{s}$  are ground-truth reference points for the given keypoint set.

## 4.2. Training Data Pre-Processing

Given a mesh  $\mathcal{M}$  with a corresponding color texture, we fit GHUM parameters using a standard 3D facial landmark based optimization for global alignment with refinement based on Iterative Closest Points (ICP) [6]. As some of the training scans belong to the same person, we further tie the parameters of the same identity  $\beta$ . We collect the sets of on-surface points  $\mathcal{O}$  and near-surface points  $\mathcal{F}$  using the procedure in [4]. To gather a set of patches  $\mathcal{P}$ , we take the following approach. First, we uniformly sample a set of points on the surface of  $\mathcal{M}$ . Next, we compute their distance to the closest facial landmark  $\mathcal{K}$ . We transform these distances into probabilities using a radial basis function (RBF) kernel followed by normalization and draw another set of candidate samples from this distribution. By

increasing the bandwidth parameter of the RBF kernel one can skew the distribution to sample more points that belong to the face region. For each point in this candidate set, we create a virtual camera looking at the sampled point along its surface normal at a fixed distance of 4 cm. We render the patch at a small resolution of  $64 \times 64$  px using orthographic projection and store the color and 3D surface location of each pixel in the patch. Finally, we select from the candidate set the top patches with most coverage, *i.e.* as few pixels associated with empty space.

## 4.3. Implementation Details

The two network branches are modeled with four 512-dimensional fully-connected layers with Swish activation [54]. We apply positional encoding [59] on  $s$  and  $g$  before passing them to the networks. The geometric identity  $\iota_g$  and appearance  $\iota_a$  are learned using 128-dimensional codes, while the  $g$  is 8-dimensional. To prevent overfitting and to obtain disentangled parameters (*cf.* Sec. 5.3), we randomly replace  $(\theta, \epsilon)$  pairs with Gaussian noise at 50% probability. Further, we start training with the  $\mathcal{L}_{\text{KL}}$  loss disabled and then linearly increase its influence. We do not follow the auto-decoder learning scheme proposed by DeepSDF where every scan is represented in each training step. Instead, we employ the standard way of training neural networks with randomly sampled batches for each update step. See our Suppl. Mat. for training details.

## 5. Experiments

We evaluate our model and its design choices by means of ablations and comparisons. In Sec. 5.1 we demonstrate the representation power and the properties of our model. We continue by comparing PhoMoH with i3DMM, a recent implicit 3D model of human heads, and ablate critical design choices. Finally we illustrate several applications enabled by our model.

**Datasets.** We train and evaluate our model on two different datasets with different characteristics. First, we rely on a dataset captured in the lab, under controlled settings. We refer to this dataset as LHS (LabHeadScans). LHS includes

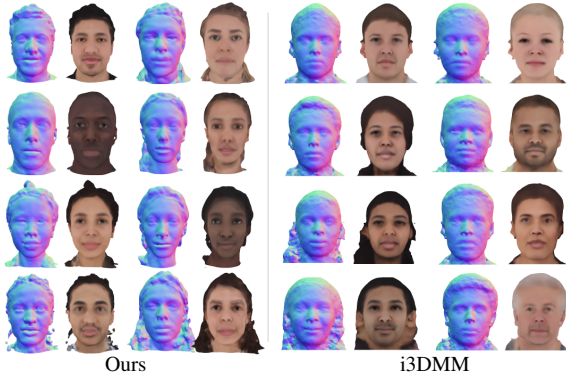


Figure 4. Random heads sampled from our model and i3DMM, trained on the RP dataset. In contrast to i3DMM, our model always matches geometry and appearance. Additionally, our results are more detailed both in geometry and color. Note that we visualize the raw, unshaded results.



Figure 5. All factors in our model are disentangled allowing for fine-grained control. Here we sample three different matching appearances for each subject, while keeping remaining factors (geometric identity, head shape, pose, expression) fixed.

scans of 200 individuals taking up to 40 different combinations of facial expressions and head poses each, totaling in 7,839 scans. All subjects have given informed consent covering the use-case presented here. Since this dataset was originally captured for building a classical mesh-based head model, the subjects are wearing caps and variation in hair styles is lacking. However, facial hair is present in the data. To demonstrate the full potential of our model, we additionally train it on as little as 100 scans purchased from RenderPeople [1], which we refer to as RP. By evaluating our method on both datasets, the rich LHD dataset and the very small but diverse RP dataset, we are able to showcase different properties and the unique strengths of PhoMoH.

**Baselines.** We compare our model with i3DMM [72], a recent implicit 3D model of human heads. In contrast to our model, i3DMM is not extending an existing head model but is learned directly from scans. i3DMM allows to control for identity, appearance, and facial expression – we additionally allow control over head pose and shape. i3DMM’s latent codes are unstructured, and thus do not allow for direct sampling. Further, i3DMM expression code is not coupled with any other model and is usually controlled by moving along the directions of the training expressions. Finally, i3DMM learns a reference shape to disentangle color from appearance. However, this leads to problems in practice, as we will show. i3DMM requires to compute gradients w.r.t. to all scans in each training step, which makes it slow and memory-intensive to train. To be able to train i3DMM we therefore had to define a new dataset LHS-40, a subset of

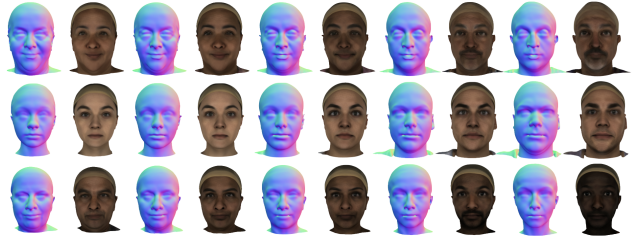


Figure 6. By enforcing a Gaussian prior on latent codes, we ensure compact, well covered latent spaces. We demonstrate this property by linearly interpolating three configuration pairs (left, right) to create plausible intermediate identities (middle).

LHS including only 40 of 200 individuals. We use LHS-40 or RP whenever comparing with i3DMM. We further compare against imGHUM [3] and FLAME [41] for the task of mesh reconstruction, and to show how PhoMoH adds benefits in representation power.

## 5.1. Representation Power

We demonstrate the representation power of PhoMoH by randomly sampling from the latent embeddings for identity, appearance, head shape, and expression. In Fig. 3 and Fig. 4 we show results for both datasets. See the Suppl. Mat. for additional results and a numerical comparison. The ability to directly sample from the latent embeddings is enabled by the Gaussian prior imposed during training. In contrast, for i3DMM one has to run PCA on the latent spaces to support sampling. Thus, sampling is performed without knowledge of the true underlying data distribution. In contrast to our results, outputs by i3DMM are less detailed and geometry and color are not always consistent. Additionally, i3DMM is learned in a normalized space, thus all samples have ambiguous scale. In contrast, PhoMoH is defined in a metric space. Geometric identity and appearance are decoupled in our model. This allows us to sample multiple plausible appearances for a given geometry, as shown in Fig. 5. Finally, we interpolate between two sampled model configurations in Fig. 6. The intermediate results are detailed and plausible, demonstrating a compact, well-covered latent space.

## 5.2. Mesh Reconstruction

One possible use case of PhoMoH, among others, is representing a scan by fitting our model to it. We compare our model on this task with i3DMM, FLAME, and imGHUM using the test set of our LHS dataset. For fair comparisons with i3DMM, as mentioned previously, we created a separate train split, LHS-40, which includes only 40 of the original scan identities. We trained both our model and i3DMM on this smaller subset. The test split contains 10 unseen identities with up to 40 expressions each and 366 scans in total. We pre-process the test split for i3DMM (canonicalizing pose, normalizing scale) and use the raw scans for all other methods. We report bidirectional Point to Sur-

	P2S ↓	Ch. ↓	NC ↑	Color ↓	LPIPS ↓
i3DMM [72]	2.009	0.322	<b>0.966</b>	<b>0.057</b>	0.140
imGHUM [3] †	2.957	0.121	0.946	–	–
FLAME [41]	1.767	<b>0.029</b>	0.945	–	–
Ours (LHS-40) †	<b>1.425</b>	0.034	<b>0.966</b>	0.069	<b>0.125</b>

Table 1. Fitting results on the LHS-40 test set. Methods with † produce an oral cavity not present in the scans, which negatively impacts the numerical results, see discussion.

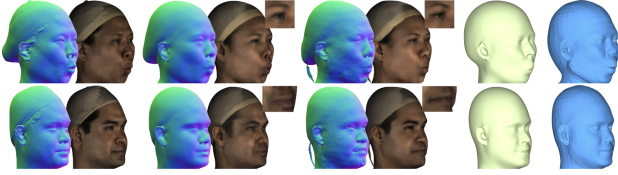


Figure 7. Qualitative comparison of fitting results. From left to right: target scan, ours, i3DMM, imGHUM, and FLAME.

face Distance (P2S) in mm, Chamfer distance ( $\times 10^{-3}$ ), and Normal Consistency (NC) for geometry reconstruction, and P2S color difference for assessing the color reconstruction quality. Additionally, we report the Learned Perceptual Image Patch Similarity [74] (LPIPS) on frontal renderings, see Tab. 1. Our geometric reconstructions are numerically more accurate than i3DMM as this occasionally features floating artifacts and discontinuities caused by their reference shape strategy. i3DMM has numerically slightly better P2S color quality, but the results appear blurry, as evident in Fig. 7 and from LPIPS results. We include imGHUM in this comparison demonstrating that most of the detail in the geometric reconstruction is recovered by the geometric identity layer of our method. imGHUM is a good proxy, but is restricted to a coarse representation of a scan. Further, we compare against FLAME, a popular mesh-based 3DMM. FLAME is high-dimensional with a shape space of 300 PCA bases and an expression space of 100 bases. In contrast, imGHUM, the model PhoMoH shares its base parameterization with, is controlled by 16 and 20-dimensional shape and expression codes, respectively. Nevertheless, FLAME produces less personalized results than PhoMoH which is evident in lower NC and P2S. FLAME reports the best results on Chamfer. This is likely because PhoMoH and imGHUM always produce a physically plausible oral cavity, even if not present in the fitted scan. This affects the Chamfer distance the most as this measures the quadratic point to point error. In summary, our method produces the best overall results and is the only method capturing sharp and realistic appearance.

### 5.3. Ablations

We ablate several important design choices: the introduction of the patch loss  $\mathcal{L}_p$ , strategies for  $(\theta, \epsilon)$  conditioning, and the normalization of the geometric feature  $g$ .

Our proposed patch loss  $\mathcal{L}_p$  significantly improves the visual fidelity of the results. See Fig. 8 (right) for a side-by-side comparison. This is also evident from a significantly

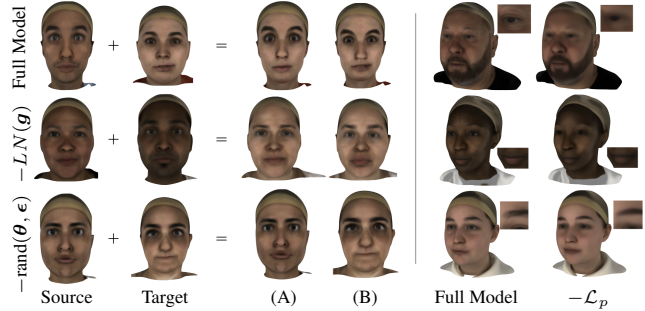


Figure 8. Ablation of critical design choices. Left: Layer normalization and randomization are essential to obtain disentanglement of model parameters. We show the source head with target appearance (A) and target appearance/pose/expression (B). Only our full model produces the desired result. Right: Our novel patch loss  $\mathcal{L}_p$  significantly increases the visual fidelity of results.

lower Frchet Inception Distance [57] (FID) compared to a model trained without  $\mathcal{L}_p$ . To compute the FID score ( $\downarrow$ ) we rendered samples of each model and compare them against renderings of real scans. Our full model has a FID score of 50.80 whereas a model without  $\mathcal{L}_p$  has a score of 80.69.

Randomly replacing pose and expression  $(\theta, \epsilon)$  pairs with Gaussian noise during training is crucial for disentangled latent representations. When  $(\theta, \epsilon)$  are always input to  $g$  and  $a$ , the networks can choose to ignore the geometry and appearance inputs  $\iota_g$  and  $\iota_a$  and partly or entirely correlate shape and appearance with  $(\theta, \epsilon)$  instead. Not using  $(\theta, \epsilon)$ , on the other hand, degrades visual fidelity (FID: 61.19). Failed disentanglement can also be observed when not applying layer normalization on the geometric feature  $g$ . We hypothesize that, without constraining the distribution of  $g$ , the network is able to leak geometric information into the appearance network which prevents proper disentanglement of  $\iota_g$  and  $\iota_a$ . In Fig. 8 (left), we show examples of such failed disentanglement along with results from our model. The appearance code lost its meaning for the example without layer normalization (line 2). Instead of applying the target appearance, the model produces a random (yet realistic) result. For the experiment without  $(\theta, \epsilon)$  randomization (line 3), we observe that appearance is correlated with pose and expression instead of being controlled with  $\iota_a$ . In contrast, our complete model produces the desired result.

### 5.4. Applications

Finally, we are demonstrating additional use-cases of PhoMoH. The per-point geometric feature  $g$  learned by our model can be understood as semantic correspondences between different head instances, see Fig. 11. This is a useful property, as we now show. First,  $g$  enables semantically correct appearance transfer between different head instances, useful for *e.g.* dataset augmentation or creative editing. We show results in Fig. 9 and compare to appearance transfer results obtained using i3DMM. While our model correctly

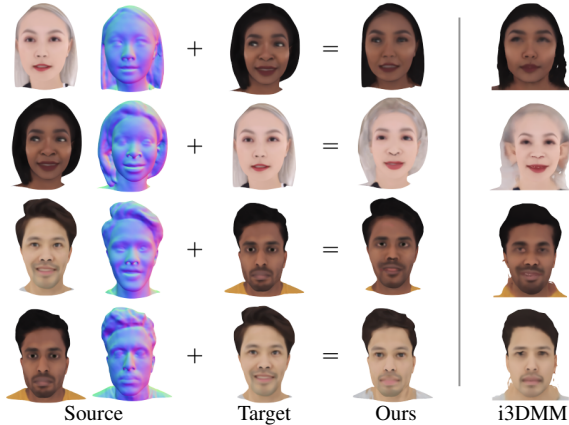


Figure 9. The proposed geometric feature enables semantically coherent appearance transfer between samples, useful for *e.g.* creative editing or dataset augmentation and diversification. From left to right: original appearance together with its geometric identity, target appearance, the result of appearance transfer, result of i3DMM [72]. Please note semantically coherent results of our method for *e.g.* hair coloring, despite different hair styles between source and target. i3DMM fails to preserve the hair line, as it is especially visible in the 2nd row (ear region).



Figure 10. By freezing the appearance code for some portions of the reconstructed mesh, and re-querying other parts, we can perform semantically coherent appearance edits. Here we sample new colors for points corresponding to the hair in the source mesh (left). Note how the model produces plausible novel hair colors.



Figure 11. Our method learns a geometric feature  $g$  (without explicit supervision) to serve as semantically informed input to the appearance network.  $g$  is a useful tool beyond its original use case as it defines dense correspondences between all sampled heads. Here we show the first 3 PCA components as RGB colors.



Figure 12. We transfer semantic labels from one head (left) to others (right) by training a classifier based on the geometric feature  $g$ . The classifier correctly predicts semantic labels for diverse heads despite being trained on a single head instance.

places colors semantically, i3DMM struggles to maintain the hair line defined by the geometry. This is especially apparent in row two, where i3DMM textures the hair region with colors from the ear region. Similar problems can be observed in Fig. 4. i3DMM’s inability to follow the seman-

tics defined by the geometry is rooted in model’s design, where learning of color is decoupled from geometry on a canonical reference shape. Our model also supports local appearance editing, as shown in Fig. 10. In this experiment, we re-queried points corresponding to hair with newly sampled appearance codes. Our model produces plausible hair colors, following the shape defined by the original hairstyle. The geometric feature is also useful for classification and segmentation tasks. In our final experiment, we labeled one single head instance with six semantic labels, corresponding to cap, eyes, ears, nose, mouth, and skin. We then trained a classifier mapping  $g$  to one of the six labels. Despite being trained only on a single head, our classifier gracefully generalizes to samples produced by PhoMoH, see Fig. 12. This means, once trained, PhoMoH can drastically simplify and speed up the labeling process for a given dataset.

## 6. Discussion & Conclusions

**Limitations.** While already modeling large parts of the human head, our model still lacks certain features for true realism. For instance, our model does not capture dynamics that may be present *e.g.* in the hair caused by motion or gravity. Furthermore, our model currently does not allow to control eye-movements and extreme expressions are somewhat limited by the expressiveness of imGHUM. Finally, PhoMoH occasionally produces blurry appearance or geometry defects.

**Ethical Considerations.** Our model is a useful tool for generating diverse instances of human heads, even when trained on relatively little data. Its unique properties allow for disentangled control over head geometry and semantically coherent appearance. Our model is not intended or particularly useful for any form of deep fakes. In order to *faithfully* represent an existing person with our model, we would need access to high-quality 3D scans of that person. While our model can be animated and realistically rendered (without audio), there is still a realism gap between our renders and real video (see limitations).

**Conclusions.** We have presented PhoMoH, a novel methodology to construct photorealistic generative 3D head models with disentangled control over geometric identity, appearance, expression, head pose, and head shape. In contrast to prior work, our implicit formulation makes it possible to model the human head as a whole, including hair and clothing. An important property of PhoMoH are the proposed per-point geometric features learned without explicit supervision. The geometric features not only ensure that appearance is coherent with the semantics defined by the geometry, but they additionally enable interesting applications such as semantic label transfer or appearance editing. In the future, we would like to add control over eye-movements as well as allow for decoupled control over the semantic regions of the head, like, for instance the hair style.



## Supplementary Material

In this supplementary material, we detail our implementation, list the values of all hyper-parameters, give inferences timings, and present additional results and experiments. Please also see the accompanying video.

### A. Implementation Details

The two network branches, for geometry and color, share the same architecture represented by 4 Dense layers with Swish activation [54] as the non-linearity. The hidden size of a Dense layer is set to 512. We set the size of both our geometric identity code  $\iota_g$  and appearance  $\iota_a$  to 128, and the size of the geometric feature code  $g$  to 8. We apply 5 and 10-dimensional positional encoding [59] on  $s$  and  $g$ , respectively, before passing them to the networks. In total, our architecture has  $\approx 1.8M$  trainable parameters.

We train for 1.5M steps, using 2 Adam optimizers, one for the network weights and one for the identity codes, respectively. For the former, the learning rate is set to  $5 \times 10^{-4}$ , while for the latter to  $1 \times 10^{-3}$ , with an exponential decay schedule (i.e. 0.8 decay every 5000 steps). For RP and LHS-40, we train only for 150k steps, to prevent overfitting on those small datasets. We train with a batch size of 256 on 16 TPUv2. Each training example consists of 512 points sampled on surface and  $2 \times 512$  around the surface. For the latter, we consider 512 samples of points closer to the surface and additional 512 points uniformly sampled in the scene bounding box. We also include one randomly selected  $64 \times 64$  px patch out of 1024 pre-computed patches for each training example in the batch. Our training weights for the losses are set to the following values:  $\lambda_n = 1.0$ ,  $\lambda_e = 0.1$ ,  $\lambda_l = 0.1$ ,  $\lambda_c = 2$ ,  $\lambda_{pc} = 1.0$ ,  $\lambda_{pd} = 5.0$ ,  $\lambda_{pp} = 0.3$ ,  $\lambda_k = 10.0$ . Further, we start training with the  $\mathcal{L}_{KL}$  loss disabled and then linearly increase it to  $\lambda_{kl} = 0.05$  over the course of the first 200k training steps. Similarly, we start with  $\lambda_g = 5.0$  and linearly increase it to  $\lambda_g = 20.0$  over 50k steps.

To prevent our networks to disregard the information in the identity codes and overfit on the GHUM parameters, we replace  $(\theta, \epsilon)$  pairs passed to  $g$  and  $a$  with Gaussian noise with 50% probability. For RP, where no per subject  $(\theta, \epsilon)$  variation is present, we disable conditioning on those factors. Finally, we also optimize the GHUM parameters together with the rest of our architecture.

### B. Inference Timings

During inference, we run Marching Cubes over the distance field defined by the geometry network  $g$ . We first discretize and probe the 3D space (represented as a rectangular cuboid centered at the origin) at a coarse resolution and then, by employing Octree sampling, we gradually raise the resolution as we come nearer to the surface. This is highly ef-

Head model	Metric	Template free (implicit)	Unstructured training data	Pose control	Appearance	Hair, Clothing	Oral cavity	
✓	✗	✓	✓	✗	✓	✓	✗	i3DMM [72]
✓	✓	✓	✗	✓	✗	✗	✓	imGHUM [3]
✓	✓	✗	✗	✓	✗ <sup>†</sup>	✗	✗	FLAME [41]
✗	✗ <sup>‡</sup>	✓	✗	n/a	✗	✗	✓	ImFace [75]
✗	✓	✗	✗	n/a	✓	✗	✗	BFM [27]
✓	✓	✓	✓	✓	✓	✓	✓	<b>PhoMoH</b>

<sup>†</sup> extension for face region proposed in [58], <sup>‡</sup> uniformly scaled space

Table 2. Overview of different features of PhoMoH and all baselines. PhoMoH is the most flexible and complete model.

fective at reducing the computational load. We query in batches of  $64^3/2$  points. As Marching Cubes produces a triangular mesh, our next step is to use its vertices to query our full network  $f$  in order to obtain per-vertex color  $c$ . The reconstruction of a colored mesh at a target resolution of  $256^3$  takes on average 1.13 seconds on an NVIDIA V100. When using a very fine resolution of  $512^3$ , the time needed increases to 5.25 seconds on average. The resultant mesh can be imported and rendered using any conventional 3D graphics software or library (e.g. Blender, Meshlab, Unreal Engine, Unity).

## C. Additional Results & Experiments

In the following, we show additional random samples taken from our models, demonstrate the usage of our model for dataset creation, and present a strategy for local geometry edits.

### C.1. Random Head Sampling

In Fig. 13, we show more randomly sampled heads using our models. In contrast to Fig. 3 and Fig. 4 in the main paper, we additionally randomize the head pose making full use of all five control parameters of our model: geometric identity, appearance, expression, head pose, and head shape. Please note that the RP dataset contains very little variation in head pose and expression, yet our model is able to produce heads with these factors varied.

Next, we numerical compare the quality of samples of our method and samples produced by our main baseline i3DMM. For a fair numerical comparison the same (ideally statistical) strategy for both methods would be required. Unfortunately, this is not possible: We sample from PhoMoH using its latent statistical model. i3DMM’s latent spaces do not define a statistical model, so “sampling” from it requires ad-hoc solutions (trading-off between quality and diversity). Nevertheless, we attempt a fair comparison here by hand-tuning sampling parameters per PCA-component



Figure 13. Random heads sampled from our models trained on the LHS (top) and RP (bottom) datasets varying all factors, namely geometric identity, appearance, expression, head pose, and head shape. For each sample, we show 3D geometry and appearance side-by-side.



Figure 14. Local geometry editing: We define local regions based on imGHUM reference points  $s$  and sample new geometric identities for points belonging to those regions. From left to right: Original geometry, appearance, region labels, four geometry and appearance pairs with locally altered geometry.

for i3DMM’s sampling strategy and transforming its results back into the metric space (results are in a canonical, non-metric space). As i3DMM cannot be trained with our full dataset (as explained in Sec. 5 Baselines) and less data leads to degraded sampling performance, we compare here with our model trained on the smaller dataset LHS-40. Like in the main paper, we rendered samples of each model and compare them against renderings of real scans to compute the FID score ( $\downarrow$ ). Our LHS-40 model has a FID score of 68.73 whereas i3DMM has a score of 81.37. While we stress again that numbers vary based on the exact sampling strategy, we conclude that our model produces more realistic images. This also correlates well with the qualitative comparisons we made in main paper. Further, our model can be trained with much more data resulting in even improved performance.

## C.2. Local Geometry Editing

The geometric identity component of PhoMoH is modeled as a layer around imGHUM. In the process of computing the signed distance of a point in space  $x$ , we compute its nearest neighbor  $s$  on the imGHUM surface. By defining local regions based on  $s$ , we can locally edit the geometric identity. In Fig. 14, we defined three semantic regions illustrated by the white label. We then we edited three scans embedded in our model, by randomly sampling geometric identity codes  $\nu_g$  for points  $x$  with the nearest neighbor of  $s$  falling into the defined region and keeping the original code otherwise.

## C.3. ImFace Comparison

ImFace [75] is an implicit 3D morphable face model with separate control over identity and expression. ImFace was trained on registered meshes from FaceScape [70] with shared topology and in a canonicalized pose. In contrast, PhoMoH can be trained with unstructured scans with vary-



Figure 15. Qualitative comparison of face fitting results. From left to right: ground truth face scan, ours, ImFace, and BFM. PhoMoH is on par with the specialized face model ImFace in terms of geometry reconstruction and is additionally able to reconstruct color and to realistically complete the full head.

	S2M $\downarrow$	UNC $\uparrow$	Color $\downarrow$
ImFace [75]	0.618	<b>0.964</b>	-
BFM [27]	1.033	0.948	0.183
Ours	<b>0.604</b>	0.956	<b>0.049</b>

Table 3. Numerical results of the face fitting experiment.

ing pose. More importantly, ImFace only models the *face geometry*, whereas PhoMoH models both the geometry and appearance of the *whole head* – a significantly harder task. A overview of different features of PhoMoH and all compared models is given in Tab. 2. Despite the different features and capabilities, we compare here with ImFace on the task of 3D fitting to scans, similar to Sec. 5.2 in the main paper. For this comparison, we processed our LHS test scans using ImFace’s cropping and pseudo watertightening algorithm. We fit both ImFace, using the official implementation, and PhoMoH to the processed scans. In contrast to the fitting experiment in the main paper, here we report unidirectional Scan to Mesh distance (S2M) and unidirectional

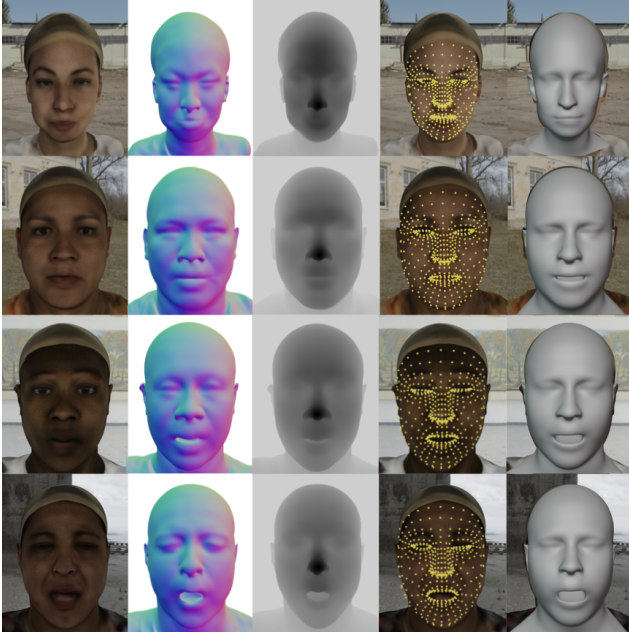


Figure 16. We can obtain various annotations for head samples from our model, making it a useful tool for dataset generation. Here we show rendered image, surface normals, depth, 3D landmarks, and the GHUM mesh.



Figure 17. Qualitative results of the 2D landmark detection model trained using heads sampled from our model.

tional Normal Consistency (UNC) as our method produces a complete head and we are only interested in evaluating the facial region. Despite comparing to a specialized face geometry model with fewer degrees of freedom, our results are on par, see Tab. 3. While ImFace only reconstructs the face geometry, PhoMoH additionally accurately reconstructs the color and is able to realistically complete the full head. See Fig. 15 for a side-by-side comparison.

In addition to ImFace, we report results for the mesh-based Basel Face Model (BFM) [27]. However, the BFM is not very diverse, especially in its appearance space as *e.g.* evident from the second row in Fig. 15. Thus, it is not well suited for a meaningful comparison on our test data and we report results only for completeness.

## C.4. Landmark Detection

The nature of our model also allows its usage for dataset generation. A number of annotations can be obtained automatically, as we show in Fig. 16. This often not the case for related image generation models, implicit representations, or neural radiance fields. Other annotations can be transferred between instances, as we have shown in the main paper. We demonstrate the usefulness of our model for dataset generation as follows. Our proposed PhoMoH model allows us to associate each sampled head with a GHUM mesh approximating its geometry. We use this property to generate a synthetic dataset of pairs of rendered images together with 468 2D landmark positions, collected from the corresponding GHUM meshes and projected into the image plane. We generate 20k samples for training and 3k samples for validation, sampling from all the disentangled factors of our model  $\mathcal{Z} = (\theta, \beta, \epsilon, \iota_g, \iota_a)$ . Additionally, we sample a random camera rotation and position from which to render over a random HDRI background [33]. We retrain the architecture of FaceMesh [30] using our synthetic dataset as sole supervision source. In Fig. 17, we show qualitative examples demonstrating that our head samples allow to train detectors that generalize well to real images.

## References

- [1] <https://renderpeople.com/>. 6
- [2] Victoria Fernández Abrevaya, Stefanie Wuhler, and Edmond Boyer. Multilinear autoencoder for 3d face model learning. In *Winter Conf. on Applications of Computer Vision*, pages 1–9. IEEE, 2018. 2
- [3] Thimo Alldieck, Hongyi Xu, and Cristian Sminchisescu. imGHUM: Implicit generative models of 3D human shape and articulated pose. In *Int. Conf. Comput. Vis.*, 2021. 1, 2, 3, 6, 7, 9
- [4] Thimo Alldieck, Mihai Zanfir, and Cristian Sminchisescu. Photorealistic monocular 3d reconstruction of humans wearing clothing. In *IEEE Conf. Comput. Vis. Pattern Recog.*, 2022. 2, 4, 5
- [5] ShahRukh Athar, Zexiang Xu, Kalyan Sunkavalli, Eli Shechtman, and Zhixin Shu. Rignrf: Fully controllable neural 3d portraits. In *IEEE Conf. Comput. Vis. Pattern Recog.*, pages 20364–20373, 2022. 3
- [6] Paul J Besl and Neil D McKay. Method for registration of 3-d shapes. In *Sensor fusion IV: control paradigms and data structures*, pages 586–606. Spie, 1992. 5
- [7] Volker Blanz and Thomas Vetter. A morphable model for the synthesis of 3d faces. In *Proc. of the 26th annual Conf. on Computer Graphics and Interactive Techniques*, pages 187–194, 1999. 1, 2
- [8] James Booth, Anastasios Roussos, Stefanos Zafeiriou, Allan Ponniah, and David Dunaway. A 3d morphable model learnt from 10,000 faces. In *IEEE Conf. Comput. Vis. Pattern Recog.*, pages 5543–5552, 2016. 2
- [9] James Booth, Epameinondas Antonakos, Stylianos Ploumpis, George Trigeorgis, Yannis Panagakis, and

- Stefanos Zafeiriou. 3d face morphable models “in-the-wild”. In *IEEE Conf. Comput. Vis. Pattern Recog.*, 2017.
- [10] James Booth, Anastasios Roussos, Allan Ponniah, David Dunaway, and Stefanos Zafeiriou. Large scale 3d morphable models. *Int. J. Comput. Vis.*, 126(2):233–254, 2018. 2
- [11] Egor Burkov, Ruslan Rakhimov, Aleksandr Safin, Evgeny Burnaev, and Victor Lempitsky. Multi-neus: 3d head portraits from single image with neural implicit functions. *arXiv preprint arXiv:2209.04436*, 2022. 2
- [12] Chen Cao, Yanlin Weng, Shun Zhou, Yiyong Tong, and Kun Zhou. Facewarehouse: A 3D facial expression database for visual computing. *IEEE Trans. Vis. Comput. Graph.*, 20(3):413–425, 2013. 2
- [13] Chen Cao, Hongzhi Wu, Yanlin Weng, Tianjia Shao, and Kun Zhou. Real-time facial animation with image-based dynamic avatars. *ACM Trans. Graph.*, 2016. 2
- [14] Chen Cao, Tomas Simon, Jin Kyu Kim, Gabe Schwartz, Michael Zollhoefer, Shun-Suke Saito, Stephen Lombardi, Shih-En Wei, Danielle Belko, Shou-I Yu, Yaser Sheikh, and Jason Saragih. Authentic volumetric avatars from a phone scan. *ACM Trans. Graph.*, 2022. 2
- [15] Eric R Chan, Connor Z Lin, Matthew A Chan, Koki Nagano, Boxiao Pan, Shalini De Mello, Orazio Gallo, Leonidas J Guibas, Jonathan Tremblay, Sameh Khamis, et al. Efficient geometry-aware 3d generative adversarial networks. In *Proceedings of the IEEE/CVF Conference on Computer Vision and Pattern Recognition*, pages 16123–16133, 2022. 3
- [16] Qifeng Chen and Vladlen Koltun. Photographic image synthesis with cascaded refinement networks. In *Proceedings of the IEEE international conference on computer vision*, pages 1511–1520, 2017. 4
- [17] Zhiqin Chen and Hao Zhang. Learning implicit fields for generative shape modeling. In *IEEE Conf. Comput. Vis. Pattern Recog.*, pages 5939–5948, 2019. 1, 2
- [18] Julian Chibane, Thiemo Alldieck, and Gerard Pons-Moll. Implicit functions in feature space for 3d shape reconstruction and completion. In *IEEE Conf. Comput. Vis. Pattern Recog.* IEEE, 2020. 2
- [19] Enric Corona, Tomas Hodan, Minh Vo, Francesc Moreno-Noguer, Chris Sweeney, Richard Newcombe, and Lingni Ma. Lisa: Learning implicit shape and appearance of hands. In *IEEE Conf. Comput. Vis. Pattern Recog.*, 2022. 2
- [20] Hang Dai, Nick Pears, William AP Smith, and Christian Duncan. A 3d morphable model of craniofacial shape and texture variation. In *Int. Conf. Comput. Vis.*, pages 3085–3093, 2017. 2
- [21] Hang Dai, Nick Pears, William Smith, and Christian Duncan. Statistical modeling of craniofacial shape and texture. *Int. J. Comput. Vis.*, 128(2):547–571, 2020. 2
- [22] Boyang Deng, JP Lewis, Timothy Jeruzalski, Gerard Pons-Moll, Geoffrey Hinton, Mohammad Norouzi, and Andrea Tagliasacchi. Neural articulated shape approximation. In *Eur. Conf. Comput. Vis.* Springer, 2020. 2
- [23] Bernhard Egger, William AP Smith, Ayush Tewari, Stefanie Wuhrer, Michael Zollhoefer, Thabo Beeler, Florian Bernard, Timo Bolkart, Adam Kortylewski, Sami Romdhani, et al. 3d morphable face models—past, present, and future. *ACM Trans. Graph.*, 39(5):1–38, 2020. 1, 2
- [24] Yao Feng, Haiwen Feng, Michael J Black, and Timo Bolkart. Learning an animatable detailed 3d face model from in-the-wild images. *ACM Trans. Graph.*, 40(4):1–13, 2021. 1, 2
- [25] Guy Gafni, Justus Thies, Michael Zollhoefer, and Matthias Nießner. Dynamic neural radiance fields for monocular 4d facial avatar reconstruction. In *IEEE Conf. Comput. Vis. Pattern Recog.*, 2021. 2, 3
- [26] Pablo Garrido, Levi Valgaerts, Chenglei Wu, and Christian Theobalt. Reconstructing detailed dynamic face geometry from monocular video. *ACM Trans. Graph.*, 32(6):158–1, 2013. 2
- [27] Thomas Gerig, Andreas Morel-Forster, Clemens Blumer, Bernhard Egger, Marcel Luthi, Sandro Schönborn, and Thomas Vetter. Morphable face models-an open framework. In *Int. Conf. on Automatic Face & Gesture Recognition*, pages 75–82. IEEE, 2018. 2, 9, 11, 12
- [28] Simon Giebenhain, Tobias Kirschstein, Markos Georgopoulos, Martin Rünz, Lourdes Agapito, and Matthias Nießner. Learning neural parametric head models. In *IEEE Conf. Comput. Vis. Pattern Recog.*, 2023. 2
- [29] Philip-William Grassal, Malte Prinzler, Titus Leistner, Carsten Rother, Matthias Nießner, and Justus Thies. Neural head avatars from monocular rgb videos. In *IEEE Conf. Comput. Vis. Pattern Recog.*, 2022. 2
- [30] Ivan Grishchenko, Artsiom Ablavatski, Yury Kartynnik, Karthik Raveendran, and Matthias Grundmann. Attention mesh: High-fidelity face mesh prediction in real-time. *arXiv preprint arXiv:2006.10962*, 2020. 12
- [31] Amos Gropp, Lior Yariv, Niv Haim, Matan Atzmon, and Yaron Lipman. Implicit geometric regularization for learning shapes. In *Int. Conf. on Mach. Learn.*, pages 3569–3579, 2020. 2, 4
- [32] Zekun Hao, Hadar Averbuch-Elor, Noah Snively, and Serge Belongie. Dualsdf: Semantic shape manipulation using a two-level representation. In *IEEE Conf. Comput. Vis. Pattern Recog.*, pages 7631–7641, 2020. 4
- [33] Poly Haven. Poly haven: The public 3d asset library. 12
- [34] Tong He, Yuanlu Xu, Shunsuke Saito, Stefano Soatto, and Tony Tung. Arch++: Animation-ready clothed human reconstruction revisited. In *Int. Conf. Comput. Vis.*, pages 11046–11056, 2021. 2
- [35] Yang Hong, Bo Peng, Haiyao Xiao, Ligang Liu, and Juyong Zhang. Headnerf: A real-time nerf-based parametric head model. In *IEEE Conf. Comput. Vis. Pattern Recog.*, 2022. 2
- [36] Hanbyul Joo, Tomas Simon, and Yaser Sheikh. Total capture: A 3d deformation model for tracking faces, hands, and bodies. In *IEEE Conf. Comput. Vis. Pattern Recog.*, pages 8320–8329, 2018. 2
- [37] Ira Kemelmacher-Shlizerman. Internet based morphable model. In *Int. Conf. Comput. Vis.*, pages 3256–3263, 2013. 2
- [38] Taras Khakhulin, Vanessa Sklyarova, Victor Lempitsky, and Egor Zakharov. Realistic one-shot mesh-based head avatars. In *Eur. Conf. Comput. Vis.*, 2022. 2
- [39] Diederik P Kingma and Max Welling. Auto-encoding variational bayes. *arXiv preprint arXiv:1312.6114*, 2013. 4, 5

- [40] Youngjoong Kwon, Dahun Kim, Duygu Ceylan, and Henry Fuchs. Neural human performer: Learning generalizable radiance fields for human performance rendering. *Adv. Neural Inform. Process. Syst.*, 34, 2021. 3
- [41] Tianye Li, Timo Bolkart, Michael J. Black, Hao Li, and Javier Romero. Learning a model of facial shape and expression from 4D scans. *ACM Trans. Graph.*, 36(6):194:1–194:17, 2017. 1, 2, 6, 7, 9
- [42] Lingjie Liu, Marc Habermann, Viktor Rudnev, Kripasindhu Sarkar, Jiatao Gu, and Christian Theobalt. Neural actor: Neural free-view synthesis of human actors with pose control. *ACM Trans. Graph.*, 2021. 3
- [43] Lars M. Mescheder, Michael Oechsle, Michael Niemeyer, Sebastian Nowozin, and Andreas Geiger. Occupancy networks: Learning 3d reconstruction in function space. In *IEEE Conf. Comput. Vis. Pattern Recog.*, pages 4460–4470, 2019. 1, 2
- [44] Marko Mihajlovic, Yan Zhang, Michael J. Black, and Siyu Tang. LEAP: Learning articulated occupancy of people. In *Proceedings IEEE/CVF Conf. on Computer Vision and Pattern Recognition (CVPR)*, 2021. 2
- [45] Marko Mihajlovic, Shunsuke Saito, Aayush Bansal, Michael Zollhoefer, and Siyu Tang. COAP: Compositional articulated occupancy of people. In *IEEE Conf. Comput. Vis. Pattern Recog.*, 2022. 2
- [46] Ben Mildenhall, Pratul P. Srinivasan, Matthew Tancik, Jonathan T. Barron, Ravi Ramamoorthi, and Ren Ng. NeRF: Representing scenes as neural radiance fields for view synthesis. In *Eur. Conf. Comput. Vis.*, 2020. 2
- [47] Jeong Joon Park, Peter Florence, Julian Straub, Richard A. Newcombe, and Steven Lovegrove. DeepSDF: Learning continuous signed distance functions for shape representation. In *IEEE Conf. Comput. Vis. Pattern Recog.*, pages 165–174, 2019. 1, 2, 4
- [48] Keunhong Park, Utkarsh Sinha, Jonathan T Barron, Sofien Bouaziz, Dan B Goldman, Steven M Seitz, and Ricardo Martin-Brualla. Nerfies: Deformable neural radiance fields. In *IEEE Conf. Comput. Vis. Pattern Recog.*, pages 5865–5874, 2021. 3
- [49] Georgios Pavlakos, Vasileios Choutas, Nima Ghorbani, Timo Bolkart, Ahmed AA Osman, Dimitrios Tzionas, and Michael J Black. Expressive body capture: 3d hands, face, and body from a single image. In *CVPR*, pages 10975–10985, 2019. 2
- [50] Pascal Paysan, Reinhard Knothe, Brian Amberg, Sami Romdhani, and Thomas Vetter. A 3d face model for pose and illumination invariant face recognition. In *IEEE Int. Conf. on advanced video and signal based surveillance*, pages 296–301. IEEE, 2009. 1, 2
- [51] Sida Peng, Yuanqing Zhang, Yinghao Xu, Qianqian Wang, Qing Shuai, Hujun Bao, and Xiaowei Zhou. Neural body: Implicit neural representations with structured latent codes for novel view synthesis of dynamic humans. In *IEEE Conf. Comput. Vis. Pattern Recog.*, 2021. 3
- [52] Stylianos Ploumpis, Haoyang Wang, Nick Pears, William AP Smith, and Stefanos Zafeiriou. Combining 3d morphable models: A large scale face-and-head model. In *IEEE Conf. Comput. Vis. Pattern Recog.*, pages 10934–10943, 2019. 2
- [53] Stylianos Ploumpis, Evangelos Ververas, Eimear O’Sullivan, Stylianos Moschoglou, Haoyang Wang, Nick Pears, William Smith, Baris Gecer, and Stefanos P Zafeiriou. Towards a complete 3d morphable model of the human head. *IEEE Trans. Pattern Anal. Mach. Intell.*, 2020. 2
- [54] Prajit Ramachandran, Barret Zoph, and Quoc V Le. Searching for activation functions. *arXiv preprint arXiv:1710.05941*, 2017. 5, 9
- [55] Eduard Ramon, Gil Triginer, Janna Escur, Albert Pumarola, Jaime Garcia, Xavier Giro-i Nieto, and Francesc Moreno-Noguer. H3D-Net: Few-shot high-fidelity 3d head reconstruction. In *Proceedings of the IEEE/CVF International Conference on Computer Vision*, pages 5620–5629, 2021. 2, 3
- [56] Shunsuke Saito, Tomas Simon, Jason Saragih, and Hanbyul Joo. PIFuHD: Multi-level pixel-aligned implicit function for high-resolution 3d human digitization. In *IEEE Conf. Comput. Vis. Pattern Recog.*, 2020. 2
- [57] Tim Salimans, Ian Goodfellow, Wojciech Zaremba, Vicki Cheung, Alec Radford, and Xi Chen. Improved techniques for training gans. *Advances in neural information processing systems*, 29:2234–2242, 2016. 7
- [58] William A. P. Smith, Alassane Seck, Hannah Dee, Bernard Tiddeman, Joshua Tenenbaum, and Bernhard Egger. A morphable face albedo model. In *Proc. of the IEEE Conference on Computer Vision and Pattern Recognition (CVPR)*, pages 5011–5020, 2020. 9
- [59] Matthew Tancik, Pratul Srinivasan, Ben Mildenhall, Sara Fridovich-Keil, Nithin Raghavan, Utkarsh Singhal, Ravi Ramamoorthi, Jonathan Barron, and Ren Ng. Fourier features let networks learn high frequency functions in low dimensional domains. In *Adv. Neural Inform. Process. Syst.*, pages 7537–7547, 2020. 5, 9
- [60] Ayush Tewari, Mohamed Elgharib, Gaurav Bharaj, Florian Bernard, Hans-Peter Seidel, Patrick Pérez, Michael Zollhoefer, and Christian Theobalt. Stylerig: Rigging stylegan for 3d control over portrait images. In *IEEE Conf. Comput. Vis. Pattern Recog.*, pages 6142–6151, 2020. 1
- [61] Justus Thies, Mohamed Elgharib, Ayush Tewari, Christian Theobalt, and Matthias Nießner. Neural voice puppetry: Audio-driven facial reenactment. In *Eur. Conf. Comput. Vis.*, pages 716–731. Springer, 2020. 1
- [62] Luan Tran and Xiaoming Liu. Nonlinear 3d face morphable model. In *IEEE Conf. Comput. Vis. Pattern Recog.*, pages 7346–7355, 2018. 2
- [63] Daoye Wang, Prashanth Chandran, Gaspard Zoss, Derek Bradley, and Paulo Gotardo. Morf: Morphable radiance fields for multiview neural head modeling. In *ACM SIGGRAPH 2022 Conference Proceedings*, pages 1–9, 2022. 2
- [64] Lizhen Wang, Zhiyua Chen, Tao Yu, Chenguang Ma, Liang Li, and Yebin Liu. Faceverse: a fine-grained and detail-controllable 3d face morphable model from a hybrid dataset. In *IEEE Conf. Comput. Vis. Pattern Recog.*, 2022. 2
- [65] Chung-Yi Weng, Brian Curless, Pratul P. Srinivasan, Jonathan T. Barron, and Ira Kemelmacher-Shlizerman. Humanerf: Free-viewpoint rendering of moving people from

- monocular video. *IEEE Conf. Comput. Vis. Pattern Recog.*, 2022. [3](#)
- [66] Erroll Wood, Tadas Baltrušaitis, Charlie Hewitt, Sebastian Dziadzio, Thomas J Cashman, and Jamie Shotton. Fake it till you make it: Face analysis in the wild using synthetic data alone. In *IEEE Conf. Comput. Vis. Pattern Recog.*, pages 3681–3691, 2021. [1](#)
- [67] Yiheng Xie, Towaki Takikawa, Shunsuke Saito, Or Litany, Shiqin Yan, Numair Khan, Federico Tombari, James Tompkin, Vincent Sitzmann, and Srinath Sridhar. Neural fields in visual computing and beyond. In *Comput. Graph. Forum*, pages 641–676, 2022. [1](#)
- [68] Hongyi Xu, Eduard Gabriel Bazavan, Andrei Zanfir, William T Freeman, Rahul Sukthankar, and Cristian Sminchisescu. GHUM & GHUML: Generative 3d human shape and articulated pose models. In *IEEE Conf. Comput. Vis. Pattern Recog.*, pages 6184–6193, 2020. [1](#), [2](#), [3](#)
- [69] Hongyi Xu, Thiemo Alldieck, and Cristian Sminchisescu. H-NeRF: Neural radiance fields for rendering and temporal reconstruction of humans in motion. In *Adv. Neural Inform. Process. Syst.*, 2021. [3](#)
- [70] Haotian Yang, Hao Zhu, Yanru Wang, Mingkai Huang, Qiu Shen, Ruigang Yang, and Xun Cao. Facescape: A large-scale high quality 3d face dataset and detailed riggable 3d face prediction. In *IEEE/CVF Conference on Computer Vision and Pattern Recognition (CVPR)*, 2020. [11](#)
- [71] Lior Yariv, Yoni Kasten, Dror Moran, Meirav Galun, Matan Atzmon, Basri Ronen, and Yaron Lipman. Multiview neural surface reconstruction by disentangling geometry and appearance. *Advances in Neural Information Processing Systems*, 33, 2020. [4](#)
- [72] Tarun Yenamandra, Ayush Tewari, Florian Bernard, Hans-Peter Seidel, Mohamed Elgharib, Daniel Cremers, and Christian Theobalt. i3dmm: Deep implicit 3d morphable model of human heads. In *IEEE Conf. Comput. Vis. Pattern Recog.*, pages 12803–12813, 2021. [2](#), [6](#), [7](#), [8](#), [9](#)
- [73] Amir Zadeh, Yao-Chong Lim, Paul Pu Liang, and Louis-Philippe Morency. Variational auto-decoder: A method for neural generative modeling from incomplete data. *arXiv preprint arXiv:1903.00840*, 2019. [4](#)
- [74] Richard Zhang, Phillip Isola, Alexei A Efros, Eli Shechtman, and Oliver Wang. The unreasonable effectiveness of deep features as a perceptual metric. In *Proceedings of the IEEE conference on computer vision and pattern recognition*, pages 586–595, 2018. [7](#)
- [75] Mingwu Zheng, Hongyu Yang, Di Huang, and Liming Chen. Imface: A nonlinear 3d morphable face model with implicit neural representations. *arXiv preprint arXiv:2203.14510*, 2022. [2](#), [9](#), [11](#)
- [76] Yufeng Zheng, Victoria Fernández Abrevaya, Marcel C. Bühler, Xu Chen, Michael J. Black, and Otmar Hilliges. I M Avatar: Implicit morphable head avatars from videos. In *IEEE Conf. Comput. Vis. Pattern Recog.*, 2022. [2](#)